Normal Distributions Transform-Based Mapping Using Scanning LiDAR Mounted on Motorcycle

Kota Matsuo, Akihiko Yoshida
Graduate School of Science and Engineering
Doshisha University
Kyotanabe, Kyoto, Japan
e-mail: {ctwd0130, ctwf0158}@mail4.doshisha.ac.jp

Masafumi Hashimoto, Kazuhiko Takahashi
Faculty of Science and Engineering
Doshisha University
Kyotanabe, Kyoto, Japan
e-mail: {mhashimo, katakaha}@mail.doshisha.ac.jp

***Abstract*—This paper presents a 3D point cloud mapping method for Global Navigation Satellite Systems (GNSS)-denied and dynamic environments using a scanning multilayer Light Detection And Ranging (LiDAR) mounted on a motorcycle. The distortion in the scan data from the LiDAR is corrected by estimating the motorcycle's pose (3D positions and attitude angles) in a period shorter than the LiDAR scan period based on the information from Normal Distributions Transform (NDT) scan matching and an Inertial Measurement Unit (IMU). The corrected scan data are mapped onto an elevation map. The static and moving scan data, which originate from static and moving objects in the environments, respectively, are classified using the occupancy grid method. Only the static scan data are applied to generate a point cloud map using NDT-based Simultaneous Localization And Mapping (SLAM). The experimental results obtained in an urban road environment demonstrate the qualitative effectiveness of the proposed method.**

Keywords—motorcycle; LiDAR; NDT-based SLAM; distortion correction; dynamic environment.

I. INTRODUCTION

In recent years, numerous studies were conducted on the active safety and autonomous driving of vehicles and personal mobility devices, while many also focused on last-mile automation by delivery robots. Important technologies from these studies include environmental map generation (mapping) [1]–[3]. In this study, we focus on mapping with a Light Detection And Ranging (LiDAR) mounted on a vehicle.

Within the domain of Intelligent Transportation Systems (ITS), maps are generated using mobile mapping systems [4]. These maps are applied to the areas of autonomous driving and active safety for automobiles in wide road environments, such as highways and motorways. In this study, we focus on environment maps for the active safety and autonomous driving of personal mobility devices and delivery robots as well as for various social services such as disaster prevention and mitigation [5][6].

In the process, we address generating 3D point cloud maps for narrow road environments, such as community roads and scenic roads in urban and mountainous areas, using LiDAR mounted on two-wheeled vehicles (e.g., bicycles and motorcycles) with higher maneuverability than four-wheeled vehicles (e.g., cars and buses). To generate 3D point cloud maps using LiDAR-based Simultaneous Localization And Mapping (SLAM), the LiDAR data captured in the sensor coordinate frame must be accurately mapped onto the world coordinate frame using the pose (i.e., position and attitude angle) information of the vehicle. Since LiDAR generally obtains data via laser scanning, all the scan data within one scan cannot be obtained at the same time when a vehicle is moving or is changing its attitude. Therefore, if such data are transformed based on the vehicle's pose at the same time, distortion appears on the environmental maps.

To reduce the distortion in the scan data, several methods were proposed [7]–[10]. Most conventional methods were aimed at correcting the distortion in the scan data from a LiDAR mounted on four-wheeled vehicles moving on flat road surfaces. To the best of our knowledge, very few studies exist that addressed distortion correction when vehicles change their poses drastically.

Thus, we proposed a Normal Distributions Transform (NDT)-based SLAM for application in Global Navigation Satellite Systems (GNSS)-denied environments using a scanning LiDAR mounted on two-wheeled vehicle that change their pose drastically [11]. The pose of the two-wheeled vehicle was calculated via NDT scan matching [12] using the LiDAR scan data obtained for each scan period. By estimating the vehicle's pose in a period shorter than the scan period via an Inertial Measurement Unit (IMU), the distortion in the scan data was corrected. The corrected scan data were applied to 3D point cloud maps. The experimental results of the road-environment mapping by a scanning LiDAR mounted on a bicycle under a zigzag motion validated the efficacy of the proposed method.

However, further improvement to our NDT-based SLAM is needed. While it was designed to be used in static environments, moving objects such as cars, buses, two-wheeled vehicles, and pedestrians exist in practical environments. The presence of moving objects in practical dynamic environments deteriorates the mapping performance. This problem can be addressed by integrating SLAM with moving-object detection. Many SLAM methods were presented for use in dynamic environments [2][13]–[15]. However, most of the methods were based on the use of a sensor mounted on a four-wheeled vehicle. SLAM with a sensor mounted on a two-wheeled vehicle in dynamic environments remains a challenging issue.

Thus, in this paper, we present an NDT-based SLAM using a scanning LiDAR mounted on a motorcycle in GNSS-denied and dynamic environments. This paper is an extension of our previous paper [15] on NDT-based SLAM, which used a scanning LiDAR mounted on a four-wheeled vehicle within

 ISBN: 978-1-61208-766-5

Figure 1. Overview of experimental bicycle.

similar environments. The rest of this paper is organized as follows. Section II describes the experimental system. Section III summarizes the scan-data mapping based on the NDT scan matching. Section IV explains the distortion correction method for the LiDAR scan data, and Section V presents the extraction method for the static scan data from the LiDAR. Section VI explains the experiments conducted to verify the proposed method, followed by the conclusions and future work in Section VII.

II. Experimental System

Figure 1 shows the overview of the motorcycle (Honda Gyro Canopy). A scanning 32-layer LiDAR (Velodyne HDL-32E) and an IMU (Xsens MTi-300) are mounted on the upper part of the motorcycle. The maximum range of the LiDAR is 70 m, the horizontal viewing angle is 360° with a resolution of 0.16°, and the vertical viewing angle is 41.34° with a resolution of 1.33°. The LiDAR provides 384 measurements (the object's 3D position and reflection intensity) every 0.55 ms (at 2° horizontal angle increments). The time that the LiDAR beam takes to complete one rotation (360°) in the horizontal direction is 100 ms, and 70,000 measurements are obtained in one rotation.

The IMU provides the attitude angles (roll and pitch angles) and the angular velocities (roll, pitch, and yaw velocities) every 10 ms with an attitude angle error of ±0.3° (typ.) and an angular velocity error of ±0.2 °/s (typ.).

In this paper, one rotation of the LiDAR beam in the horizontal direction (360°) is referred to as one scan, while the data obtained from this scan is referred to as scan data. The LiDAR's scan period (100 ms) is denoted as τ and the scan data observation period (0.55 ms) as $\Delta\tau$. The observation period (10 ms) of the IMU is denoted as $\Delta\tau_{IMU}$, which means the IMU data are obtained 10 times in one scan of the LiDAR ($\tau = 10\Delta\tau_{IMU}$), while the LiDAR scan data are obtained 18 times within the observation period of the IMU ($\Delta\tau_{IMU} = 18\Delta\tau$).

III. Normal Distributions Transform Scan Matching

The scan data mapping is based on NDT scan matching [12]. For clarity, we explain the NDT scan matching using the LiDAR scan data in which the distortion is corrected. The distortion correction method is detailed in the following section.

A voxel grid filter is applied to downsize the scan data. The voxel used for the filter is a tetrahedron with a side length of 0.2 m. In the world coordinate frame, Σ_W , a voxel map with a voxel size of 1 m is used for NDT scan matching. For the i-th (i = 1, 2, …n) measurement in the scan data, the position vector in Σ_b is defined as $\boldsymbol{p}_{bi}$ and that in Σ_W as $\boldsymbol{p}_i$. Thus, the relation is given by the following homogeneous form:

$$\begin{pmatrix} \boldsymbol{p}_i \\ 1 \end{pmatrix} = \boldsymbol{T}(\boldsymbol{X}) \begin{pmatrix} \boldsymbol{p}_{bi} \\ 1 \end{pmatrix} \tag{1}$$

where $\boldsymbol{X} = (x, y, z, \phi, \theta, \psi)^T$ is the motorcycle's pose, $(x, y, z)^T$ and $(\phi, \theta, \psi)^T$ are the 3D position and attitude angle (roll, pitch, and yaw angles) of the motorcycle, respectively, in Σ_W . $\boldsymbol{T}(\boldsymbol{X})$ is the following homogeneous transformation matrix:

$$T(\boldsymbol{X}) = \begin{pmatrix} \cos\theta\cos\psi & \sin\phi\sin\theta\cos\psi - \cos\phi\sin\psi & \cos\phi\sin\theta\cos\psi + \sin\phi\sin\psi & x \\ \cos\theta\sin\psi & \sin\phi\sin\theta\sin\psi + \cos\phi\cos\psi & \cos\phi\sin\theta\sin\psi - \sin\phi\cos\psi & y \\ -\sin\theta & \sin\phi\cos\theta & \cos\phi\cos\theta & z \\ 0 & 0 & 0 & 1 \end{pmatrix}$$

The scan data obtained at the current time $t\tau$ (t = 0, 1, 2, …), $\boldsymbol{P}_{b(t)} = \{\boldsymbol{p}_{b1(t)}, \boldsymbol{p}_{b2(t)}, \cdots, \boldsymbol{p}_{bn(t)}\}$ or $\boldsymbol{P}_{(t)} = \{\boldsymbol{p}_{1(t)}, \boldsymbol{p}_{2(t)}, \cdots, \boldsymbol{p}_{n(t)}\}$, are referred to as the new input scan, and the scan data obtained in the previous time before $(t-1)\tau$, $\boldsymbol{P} = \{\boldsymbol{P}_{(0)}, \boldsymbol{P}_{(1)}, \cdots, \boldsymbol{P}_{(t-1)}\}$, are referred to as the reference scan.

NDT scan matching involves conducting an NDT for the reference scan data in each grid on a voxel map and calculating the mean and covariance of the LiDAR measurement positions. By matching the new input scan at $t\tau$ with the reference scan data obtained prior to $(t-1)\tau$, the motorcycle's pose $\boldsymbol{X}_{(t)}$ at $t\tau$ can be determined. The motorcycle's pose is used for conducting a coordinate transform with (1), the new input scan can then be mapped to Σ_W, and the reference scan is updated.

In this study, we use the point cloud library for the NDT scan matching [16].

IV. Distortion Correction of LiDAR Scan Data

A. Motion and Measurement Models

As shown in Figure 2, the linear velocity of the motorcycle in Σ_b is denoted as V_b (the velocity in the x_b-axis direction), and the angular velocities around the x_b-, y_b-, and z_b-axes are denoted as $\dot{\phi}_b$, $\dot{\theta}_b$, and $\dot{\psi}_b$, respectively.

If the motorcycle is assumed to move at nearly constant linear and angular velocities, a motion model can be derived as (A.1) in the Appendix. We express (A.1) in the following vector form:

$$\boldsymbol{\xi}_{(t+1)} = \boldsymbol{f}\left[\boldsymbol{\xi}_{(t)}, \boldsymbol{w}, \tau\right] \tag{2}$$

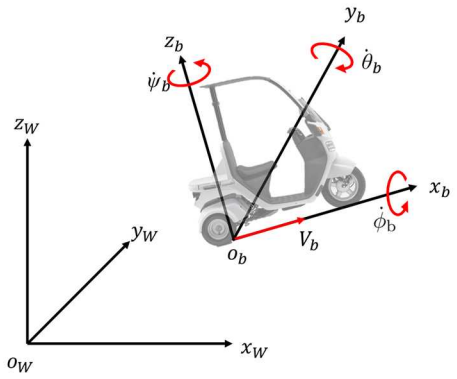

Figure 2. Notation related to motorcycle motion.

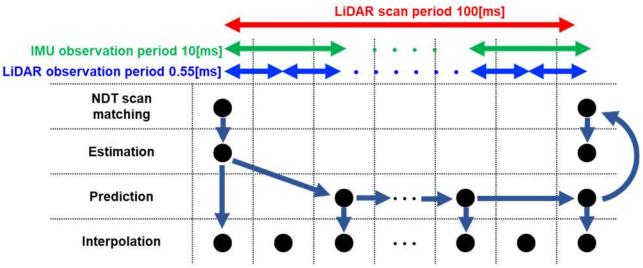

Figure 3. Flow of distortion correction.

The attitude angle and angular velocity of the motorcycle obtained at time $t\tau_{IMU}$ by the IMU is denoted as $z_{IMU}(t)$. The measurement model is then

$$z_{IMU}(t) = \boldsymbol{H}_{IMU}\xi(t) + \Delta z_{IMU}(t) \tag{3}$$

where Δz_{IMU} is sensor noise, and $\boldsymbol{H}_{IMU}$ is a measurement matrix.

The motorcycle's pose obtained at $t\tau$ using the NDT scan matching is denoted as $z_{NDT(t)} \equiv \hat{\boldsymbol{X}}_{(t)}$. The measurement model is then

$$z_{NDT}(t) = \boldsymbol{H}_{NDT}\xi(t) + \Delta z_{NDT}(t) \tag{4}$$

where Δz_{NDT} is the measurement noise, and $\boldsymbol{H}_{NDT}$ is the measurement matrix.

B. Distrotion Correction

Figure 3 shows the correction flow of the LiDAR scan data [11]. The LiDAR's scan period τ is 100 ms, the observation period $\Delta\tau_{IMU}$ of the IMU is 10 ms, and the scan data observation period $\Delta\tau$ is 0.55 ms. When the scan data are mapped onto Σ_W using the motorcycle's pose, which is calculated for every LiDAR scan period, distortion appears on the environmental map. Therefore, the distortion in the LiDAR scan data is corrected by estimating the motorcycle's pose using the Extended Kalman Filter (EKF) for every scan data observation period $\Delta\tau$.

The IMU data are obtained 10 times per LiDAR scan ($\tau = 10\Delta\tau_{IMU}$). The state estimate of the motorcycle and its error covariance obtained at the time $(t-1)\tau+(k-1)\Delta\tau_{IMU}$, where k =1–10, using EKF are denoted as $\hat{\xi}^{(k-1)}{}_{(t-1)}$ and $\boldsymbol{\Gamma}^{(k-1)}{}_{(t-1)}$, respectively. From these estimates, the EKF prediction algorithm gives the state prediction $\hat{\xi}^{(k/k-1)}{}_{(t-1)}$ and the error covariance $\boldsymbol{\Gamma}^{(k/k-1)}{}_{(t-1)}$ at $(t-1)\tau+k\Delta\tau_{IMU}$ by

$$\left.\begin{aligned}\hat{\xi}^{(k/k-1)}(t-1) &= \boldsymbol{f}[\hat{\xi}^{(k-1)}(t-1), 0, \Delta\tau_{IMU}] \\ \boldsymbol{\Gamma}^{(k/k-1)}(t-1) &= \boldsymbol{F}(t-1)\boldsymbol{\Gamma}^{(k-1)}(t-1)\boldsymbol{F}(t-1)^T + \boldsymbol{G}(t-1)\boldsymbol{Q}\boldsymbol{G}(t-1)^T\end{aligned}\right\} \tag{5}$$

where $\boldsymbol{F} = \partial\boldsymbol{f}/\partial\hat{\boldsymbol{\xi}}$, $\boldsymbol{G} = \partial\boldsymbol{f}/\partial\boldsymbol{w}$, and $\boldsymbol{Q}$ is the covariance matrix of the plant noise $\boldsymbol{w}$.

At $(t-1)\tau + k\Delta\tau_{IMU}$, the attitude angle and angular velocity z_{IMU} of the motorcycle are observed with the IMU. Then, the EKF estimation algorithm gives the state estimate $\hat{\xi}^{(k)}{}_{(t-1)}$ and its error covariance $\boldsymbol{\Gamma}^{(k)}{}_{(t-1)}$ as follows:

$$\left.\begin{aligned}\hat{\xi}^{(k)}(t-1) &= \hat{\xi}^{(k/k-1)}(t-1) + \boldsymbol{K}\{z_{IMU} - \boldsymbol{H}_{IMU}\hat{\xi}^{(k/k-1)}(t-1)\} \\ \boldsymbol{\Gamma}^{(k)}(t-1) &= \boldsymbol{\Gamma}^{(k/k-1)}(t-1) - \boldsymbol{K}\boldsymbol{H}_{IMU}\boldsymbol{\Gamma}^{(k/k-1)}(t-1)\end{aligned}\right\} \tag{6}$$

where $\boldsymbol{K} = \boldsymbol{\Gamma}^{(k/k-1)}{}_{(t-1)}\boldsymbol{H}_{IMU}^T\boldsymbol{S}^{-1}{}_{(t-1)}$ and $\boldsymbol{S} = \boldsymbol{H}_{IMU}\boldsymbol{\Gamma}^{(k/k-1)}{}_{(t-1)}\boldsymbol{H}_{IMU}^T + \boldsymbol{R}_{IMU}$. $\boldsymbol{R}_{IMU}$ is the covariance matrix of the sensor noise Δz_{IMU}.

In the state estimate $\hat{\xi}^{(k)}{}_{(t-1)}$, the elements related to the motorcycle's pose $(x, y, z, \phi, \theta, \psi)$ are denoted as $\hat{\boldsymbol{X}}^{(k)}{}_{(t-1)}$. Since the observation period $\Delta\tau_{IMU}$ of the IMU is 10 ms, and the scan data observation period $\Delta\tau$ is 0.55 ms, the LiDAR scan data are obtained 18 times within the IMU observation period ($\Delta\tau_{IMU} = 18\Delta\tau$). Using the pose estimates $\hat{\boldsymbol{X}}^{(k-1)}{}_{(t-1)}$ and $\hat{\boldsymbol{X}}^{(k)}{}_{(t-1)}$ obtained at $(t-1)\tau + (k-1)\Delta\tau_{IMU}$ and $(t-1)\tau + k\Delta\tau_{IMU}$, respectively, the motorcycle's pose $\hat{\boldsymbol{X}}^{(k-1)}{}_{(t-1,j)}$ at $(t-1)\tau + (k-1)\Delta\tau_{IMU} + j\Delta\tau$, where j = 1–18, can be interpolated by

$$\hat{\boldsymbol{X}}^{(k-1)}(t-1, j) = \hat{\boldsymbol{X}}^{(k-1)}(t-1) + \frac{\hat{\boldsymbol{X}}^{(k)}(t-1) - \hat{\boldsymbol{X}}^{(k-1)}(t-1)}{\Delta\tau_{IMU}} j\Delta\tau \tag{7}$$

Using (1) and the pose prediction $\hat{\boldsymbol{X}}^{(k-1)}{}_{(t-1,j)}$, the scan data $\boldsymbol{p}_{bi}^{(k-1)}{}_{(t-1,j)}$ in Σ_b obtained at $(t-1)\tau + (k-1)\Delta\tau_{IMU} + j\Delta\tau$ can be transformed to $\boldsymbol{p}_i^{(k-1)}{}_{(t-1,j)}$ in Σ_W as follows:

$$\begin{pmatrix}\boldsymbol{p}_i^{(k-1)}(t-1, j) \\ 1\end{pmatrix} = T(\hat{\boldsymbol{X}}^{(k-1)}(t-1, j))\begin{pmatrix}\boldsymbol{p}_{bi}^{(k-1)}(t-1, j) \\ 1\end{pmatrix} \tag{8}$$

Since the IMU data are obtained 10 times per LiDAR scan ($\tau = 10\Delta\tau_{IMU}$), the time $t\tau$ is equal to (t-1) $\tau + 10\Delta\tau_{IMU}$. Using the motorcycle's pose estimate $\hat{\boldsymbol{X}}^{(10)}{}_{(t-1)}$ at $t\tau$, the scan data $\boldsymbol{p}_i^{(k-1)}{}_{(t-1,j)}$ in Σ_W at $(t-1)\tau + (k-1)\Delta\tau_{IMU} + j\Delta\tau$ are transformed to the scan data $\boldsymbol{P}_{bi}^*{}_{(t)}$ in Σ_b at $t\tau$ by

$$\begin{pmatrix}\boldsymbol{p}_{bi}^*(t) \\ 1\end{pmatrix} = T(\hat{\boldsymbol{X}}^{(10)}(t-1))^{-1}\begin{pmatrix}\boldsymbol{p}_i^{(k-1)}(t-1, j) \\ 1\end{pmatrix} \tag{9}$$

In such way, the corrected scan data $\boldsymbol{P}_b^*{}_{(t)} = \{\boldsymbol{p}_{b1}^*{}_{(t)}, \boldsymbol{p}_{b2}^*{}_{(t)}, \cdots, \boldsymbol{p}_{bn}^*{}_{(t)}\}$ within one scan (LiDAR beam

 ISBN: 978-1-61208-766-5

rotation of 360° in a horizontal plane) are obtained and used as the new input scan for the scan matching to calculate the pose z_{NDT} of the motorcycle at $t\tau$. Then, the EKF estimation algorithm is used to calculate the state estimate $\hat{\xi}_{(t)}$ and its error covariance $\Gamma_{(t)}$ of the motorcycle at $t\tau$ as follows:

$$\left.\begin{aligned}\hat{\xi}(t) &= \hat{\xi}^{(10)}(t-1) + K(t)\{z_{NDT}(t) - H_{NDT}\hat{\xi}^{(10)}(t-1)\}\\ \Gamma(t) &= \Gamma^{(10)}(t-1) - K(t)H_{NDT}\Gamma^{(10)}(t-1)\end{aligned}\right\} \quad (10)$$

where, $K_{(t)} = \Gamma^{(10)}{}_{(t-1)} H^{T}_{NDT} S^{-1}{}_{(t)}$, $S_{(t)} = H_{NDT}\Gamma^{(10)}{}_{(t-1)} H^{T}_{NDT} + R_{NDT}$, and R_{NDT} is the covariance matrix of Δz_{NDT} .

The corrected scan data $P^{*}_{b}{}_{(t)}$ are mapped onto Σ_W using the pose estimate calculated by (10), and the distortion in the environmental maps can then be removed.

V. Removal of Moving Scan Data

In dynamic environments where moving objects such as cars, motorcycles, and pedestrians exist, the LiDAR scan data related to moving objects (referred to as moving scan data) must be removed from the entire scan data, and only the scan data related to static objects (static scan data), such as buildings and trees, have to be utilized for the mapping.

We previously studied moving-object detection and tracking in crowded environments [17][18]. This method is applied to extract the static scan data from the LiDAR scan data.

To extract the static scan data, the LiDAR scan data are first classified into two types, scan data originating from road surfaces (road-surface scan data) and scan data originating from objects (object scan data), according to a rule-based method. The object scan data obtained in Σ_b are mapped onto an elevation map represented in Σ_W using the motorcycle's pose calculated by (1). In this study, the cell of the elevation map is a square with a side length of 0.3 m.

A cell containing scan data is referred to as an occupied cell. For moving scan data, the time to occupy the same cell is short, while for static scan data, the time is long. Therefore, using the occupancy grid method based on the cell occupancy time [17], the occupied cells are classified into two types of cell, moving and static, which are occupied by the moving and static scan data, respectively. Cells that the LiDAR cannot identify due to obstructions are defined as unknown cells, and their cell occupancy time is not counted.

Since the scan data related to an object generally occupy multiple cells, adjacent occupied cells are clustered. Then, the scan data in clustered static cells are applied to the mapping.

When moving objects such as vehicles pause (e.g., at a red light), the occupancy grid-based method often misidentifies their scan data as static scan data. To address this problem, the road-surface scan data are mapped onto the elevation map, and the cells in which the road-surface scan data are occupied for a while are regarded as the road-surface cells. If the road-surface cells contain the object scan data, the object scan data are always determined as moving scan data and are removed from the entire scan data.

VI. Experimental Results

Mapping experiments were conducted within road traffic environments (Figure 4). Figure 5 shows photos of areas 1 and 2, which are shown in Figure 4. The traveled distance of the motorcycle was around 2,886 m, while its maximum speed was 30 km/h. The motorcycle turned left six times and then tilted approximately 10° in a roll direction.

Figure 4. Moved path of vehicle (top view).

(a) Area 1

(b) Area 2

Figure 5. Photo of environment.

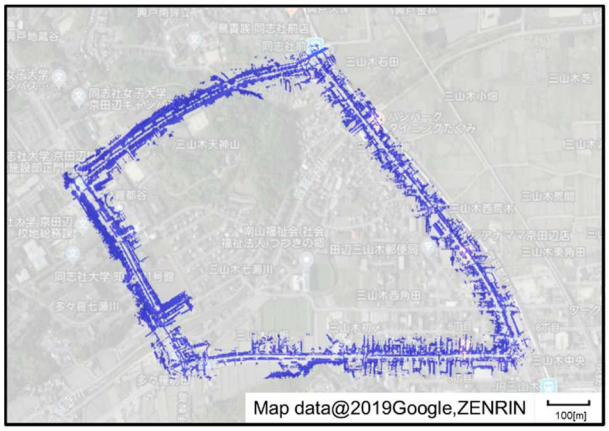

Figure 6. Mapping result (top view).

 ISBN: 978-1-61208-766-5

(a) Photo

(b) Case 1

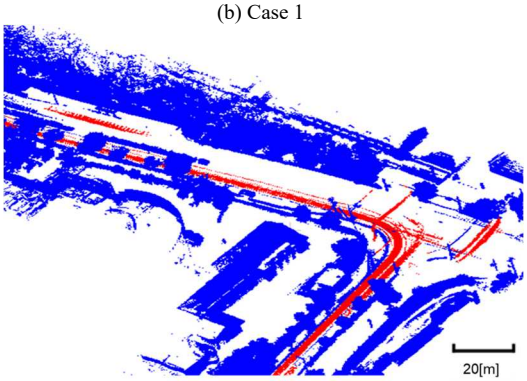

(c) Case 2

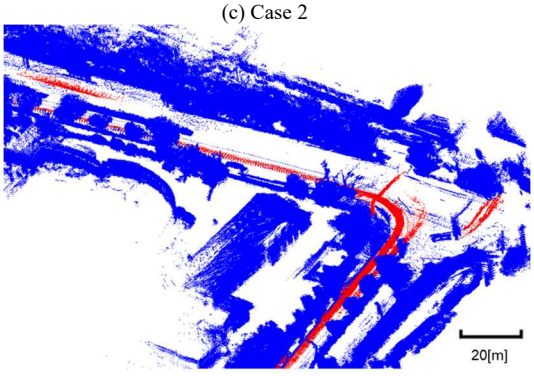

(d) Case 3

Figure 7. Mapping result of area 1 (bird's-eye view). The red line in (a) indicates the movement path of the motorcycle. The blue and red dots in (b)–(d) indicate the static and moving scan data, respectively.

(a) Photo

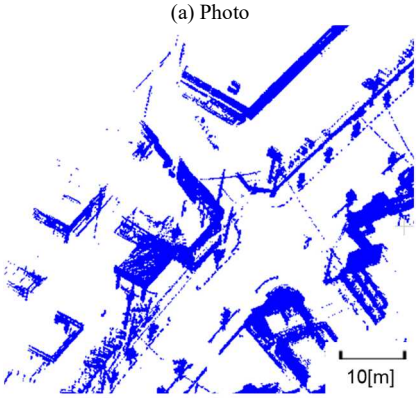

(b) Case 1

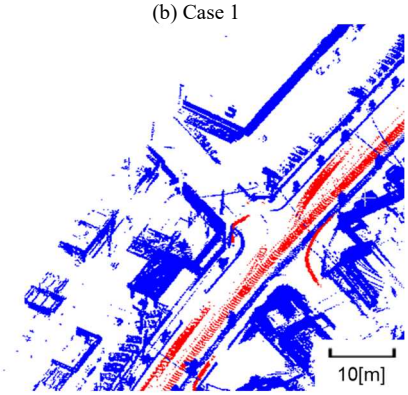

(c) Case 2

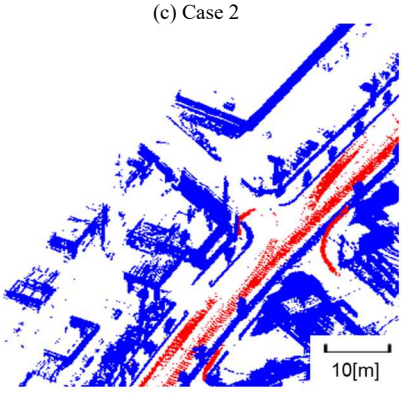

(d) Case 3

Figure 8. Mapping result of area 2 (bird's-eye view). The red line in (a) indicates the movement path of the motorcycle. The blue and red dots in (b)–(d) indicate the static and moving scan data, respectively.

 ISBN: 978-1-61208-766-5

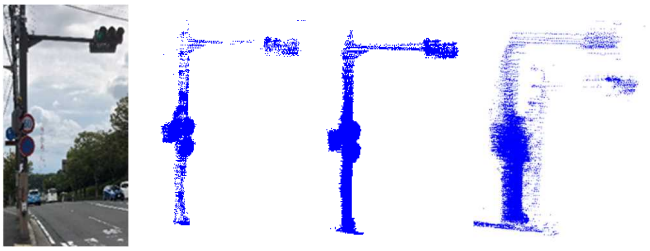

(a) Photo (b) Case 1 (c) Case 2 (d) Case 3

Figure 9. Mapping result of a traffic signal in area 1.

Figure 6 shows the mapping result using NDT-based SLAM in conjunction with distortion correction of the LiDAR scan data and the extraction of the static scan data.

To evaluate the mapping performance in detail, enlarged maps of areas 1 and 2 in Figure 4 are compiled, as shown in Figures 7 and 8. Figure 7 presents the map when the motorcycle is turning left, while Figure 8 presents the map when the motorcycle is going straight. Figure 9 also shows the mapping result of a traffic sign in area 1, in which the motorcycle is turning left. In area 1, there are four cars and four pedestrians, and in area 2, there are four cars and three pedestrians.

For comparison purposes, the maps were generated in terms of the following cases:

Case 1: Mapping by the proposed method: NDT-based SLAM with the distortion correction of the LiDAR scan data and the extraction of the static scan data from the entire LiDAR scan data.

Case 2: NDT-based SLAM with the distortion correction but without the extraction of the static scan data.

Case 3: NDT-based SLAM without either method.

As Figures 7 and 8 show, case 1 (proposed method) removes the track (red dots) of any moving objects (cars and pedestrians) more than cases 2 and 3. Meanwhile, as Figure 9 shows, the mapping results obtained in case 1 are more crisp than those obtained in case 3. Thus, the conclusion exists that the proposed method provides a better mapping result than cases 2 and 3.

However, our method of moving-object detection exhibits one drawback. When, for example, cars slow down at an intersection, stop at a red light, or pause to turn left (or right), they are sometimes determined as static objects. Then, the LiDAR scan data that relate to cars partially remain on the mapping.

VII. Conclusions and Future Work

This paper presented NDT-based mapping using a scanning LiDAR mounted on a motorcycle in GNSS-denied and dynamic environments. The distortion in the LiDAR scan data was corrected based on the information from the NDT scan matching and the IMU via EKF. The moving scan data were removed from the entire LiDAR scan data using the occupancy grid-based method, and the static scan data were applied to 3D point cloud maps using the NDT scan matching. The efficacy of the mapping was qualitatively demonstrated through experimental results obtained in road environments. We are currently conducting quantitative evaluations of the presented method in various environments.

Some improvements to the presented method are required. Since the distortion correction of the LiDAR scan data requires a great deal of computational time, Graphical Processing Unit (GPU) must be utilized in real-time operations. NDT-based SLAM degrades the mapping accuracy over time due to the accumulation error and must be integrated with Graph-based SLAM to reduce the drift. In addition, NDT-based SLAM with moving-object detection should be extended to SLAM with Detection And Tracking of Moving Objects (DATMO) for advanced rider assist systems. The SLAM DATMO approach will improve the mapping performance of both the mapping and the moving-object tracking.

Appendix: Motion Model of Motorcycle

$$\begin{pmatrix} x_{(t+1)} \\ y_{(t+1)} \\ z_{(t+1)} \\ \phi_{(t+1)} \\ \theta_{(t+1)} \\ \psi_{(t+1)} \\ V_{b(t+1)} \\ \dot{\phi}_{b(t+1)} \\ \dot{\theta}_{b(t+1)} \\ \dot{\psi}_{b(t+1)} \end{pmatrix} = \begin{pmatrix} x_{(t)} + a_{1(t)}\cos\theta_{(t)}\cos\psi_{(t)} \\ y_{(t)} + a_{1(t)}\cos\theta_{(t)}\sin\psi_{(t)} \\ z_{(t)} - a_{1(t)}\sin\theta_{(t)} \\ \phi(t) + a_2(t) + \{a_3(t)\sin\phi(t) + a_4(t)\cos\phi(t)\}\tan\theta(t) \\ \theta(t) + \{a_3(t)\cos\phi(t) - a_4(t)\sin\phi(t)\} \\ \psi(t) + \{a_3(t)\sin\phi(t) + a_4(t)\cos\phi(t)\}\dfrac{1}{\cos\theta(t)} \\ V_{b(t)} + \tau w_{\dot{V}_b} \\ \dot{\phi}_{b(t)} + \tau w_{\ddot{\phi}_b} \\ \dot{\theta}_{b(t)} + \tau w_{\ddot{\theta}_b} \\ \dot{\psi}_{b(t)} + \tau w_{\ddot{\psi}_b} \end{pmatrix} \quad \text{(A.1)}$$

where (x, y, z) and (ϕ, θ, ψ) are the 3D position and attitude angle (roll, pitch, and yaw angles) of the motorcycle, ($\dot{\phi}_b$, $\dot{\theta}_b$, $\dot{\psi}_b$) are the angular velocities (roll, pitch, and yaw velocities) of the motorcycle, and ($w_{\dot{V}_b}, w_{\ddot{\phi}_b}, w_{\ddot{\theta}_b}, w_{\ddot{\psi}_b}$) are the acceleration disturbances. $a_1 = V_b\tau + \tau^2 w_{\dot{V}_b}/2$, $a_2 = \dot{\phi}_b\tau + \tau^2 w_{\ddot{\phi}_b}/2$, $a_3 = \dot{\theta}_b\tau + \tau^2 w_{\ddot{\theta}_b}/2$, and $a_4 = \dot{\psi}_b\tau + \tau^2 w_{\ddot{\psi}_b}/2$.

Acknowledgment

This study was partially supported by the KAKENHI Grant #18K04062, the Japan Society for the Promotion of Science (JSPS).

References

[1] C. Cadena et al., "Past, Present, and Future of Simultaneous Localization and Mapping: Toward the Robust-Perception Age," IEEE Trans. on Robotics, vol. 32, pp. 1309–1332, Dec. 2016, doi: 10.1109/TRO.2016.2624754.

[2] G. Bresson, Z. Alsayed, L. Yu, and S. Glaser, "Simultaneous Localization And Mapping: A Survey of Current Trends in Autonomous Driving," IEEE Trans. on Intelligent Vehicles, vol. 2, pp. 194–220, Sept. 2017, doi: 10.1109/TIV.2017.2749181.

[3] B. Huang, J. Zhao, and J. Liu, "A Survey of Simultaneous Localization and Mapping," eprint arXiv:1909.05214, 2019.

 ISBN: 978-1-61208-766-5

[4] H. G. Seif and X. Hu, "Autonomous Driving in the iCity—HD Maps as a Key Challenge of the Automotive Industry," Engineering, vol. 2, pp.159–162, June 2016, doi:10.1016/ J.ENG.2016.02.010.

[5] K. Morita, M. Hashimoto, and K. Takahashi, "Point-Cloud Mapping and Merging using Mobile Laser Scanner," Proc. of the third IEEE Int. Conf. on Robotic Computing (IRC 2019), pp.417–418, March 2019, doi: 10.1109/IRC.2019.00078.

[6] D. Schwesinger, A. Shariati, C. Montella, and J. Spletzer, "A Smart Wheelchair Ecosystem for Autonomous Navigation in Urban Environments," Autonomous Robot, vol. 41, pp. 519–538, March 2017, doi: 10.1007/s10514-016-9549-1.

[7] S. Hong, H. Ko, and J. Kim, "VICP: Velocity Updating Iterative Closest Point Algorithm," Proc. of 2010 IEEE Int. Conf. on Robotics and Automation (ICRA 2010), pp. 1893–1898, May 2010, doi: 10.1109/ROBOT.2010.5509312.

[8] F. Moosmann and C. Stiller, "Velodyne SLAM," Proc. of IEEE Intelligent Vehicles Symp. (IV2011), pp. 393–398, July 2011, doi: 10.1109/IVS.2011.5940396.

[9] J. Zhang and A. Singh, "LOAM: Lidar Odometry and Mapping in Real-time," Proc. of Robotics: Science and Systems, Jan. 2014.

[10] K. Inui, M. Morikawa, M. Hashimoto, and K. Takahashi, "Distortion Correction of Laser Scan Data from In-Vehicle Laser Scanner Based on Kalman Filter and NDT Scan Matching," Proc. of the 14th Int. Conf. on Informatics in Control, Automation and Robotics (ICINCO), pp. 329–334, 2017, doi: 10.5220/0006422303290334.

[11] K. Tokorodani, M. Hashimoto, Y. Aihara, and K. Takahashi, "Point-Cloud Mapping Using Lidar Mounted on Two-Wheeled Vehicle Based on NDT Scan Matching," Proc. of the 18th Int. Conf. on Informatics in Control, Automation and Robotics (ICINCO), pp. 446–452, 2019, doi: 10.5220/ 00079462044 60452.

[12] P. Biber and W. Strasser, "The Normal Distributions Transform: A New Approach to Laser Scan Matching," Proc. of IEEE/RSJ Int. Conf. on Intelligent Robots and Systems (IROS 2003), pp. 2743–2748, Oct. 2003, doi: 10.1109/ IROS.2003.1249285.

[13] J. P. Saarinen, H. Andreasson, T. Stoyanov, and A. J. Lilienthal, "3D Normal Distributions Transform Occupancy Maps: An Efficient Representation for Mapping in Dynamic Environments," Int. J. of Robotics Research, vol.32, pp.1627–1644, Sept. 2013, doi:10.1177/0278364913499415.

[14] X. Ding, Y. Wang, H. Yin, L. Tang, and R. Xiong, "Multi-Session Map Construction in Outdoor Dynamic Environment," Proc. of the 2018 IEEE Int. Conf. on Real-time Computing and Robotics (IRC2018), pp. 384–389, Aug. 2018, doi: 10.1109/ RCAR.2018.8621770.

[15] M. Yamaji, S. Tanaka, M. Hashimoto, and K. Takahashi, "Point Cloud Mapping Using Only Onboard Lidar in GNSS Denied and Dynamic Environments," Proc. of the Fifteenth Int. Conf. on Systems (ICONS 2020), Feb. 2020.

[16] R. B. Rusu and S. Cousins, "3D is Here: Point Cloud Library (PCL)," Proc. of 2011 IEEE Int. Conf. on Robotics and Automation (ICRA 2011), 2011.

[17] S. Sato, M. Hashimoto, M. Takita, K. Takagi, and T. Ogawa, "Multilayer Lidar-Based Pedestrian Tracking in Urban Environments," Proc. of IEEE Intelligent Vehicles Symp. (IV2010), pp. 849–854, June 2010, doi: 10.1109/IVS.2010. 5548135.

[18] S. Kanaki et al., "Cooperative Moving-Object Tracking with Multiple Mobile Sensor Nodes -Size and Posture Estimation of Moving Objects using In-Vehicle Multilayer Laser Scanner-," Proc. of 2016 IEEE Int. Conf. on Industrial Technology (ICIT 2016), pp. 59–64, March 2016, doi: 10.1109/ICIT.2016. 7474726.

 ISBN: 978-1-61208-766-5